Self-decoration of Barium Titanate with Rhodium-NP via a facile co-precipitation route for NO sensing in hot gas environment.

Roussin Lontio Fomekong, [a,b]* Shujie You, [c] Robert Frohnhoven,[d] Tim Ludwig ,[d] Mathur Sanjay,[d] Bilge Saruhan [b]

[a] Higher Teacher Training College, University of Yaounde I, P.O.BOX 47 Yaounde, Cameroon
[b] Department of High-Temperature and Functional Coatings, Institute of Materials Research, German Aerospace Center (DLR), 51147 Cologne, Germany. Email: lonforou@yahoo.fr
[c] Division of Materials Science, Department of Engineering Sciences and Mathematics, Luleå University of technology, 97187 Luleå, Sweden
[d] Institute of Inorganic Chemistry, University of Cologne, Greinstraße 6, 50939 Cologne, Germany

Abstract:

There is an urgent need to develop real-time gas sensors capable of detection under hot-gas (> 400 °C) flow, for instance, to control exhaust emissions. In this context, Rh-doped $BaTiO_3$ has been prepared by co-precipitation route and heat-treated at 900 °C under 2% hydrogen to obtain in-situ Rh-nanoparticle decoration of submicron $BaTiO_3$ powder. X-ray diffraction, Raman, and X-Ray photoelectron spectrometry analysis confirm the presence of Barium Titanate phases and the substitution of Ti^{4+} by Rh^{3+}. According to the analytic evidence, thermal hydrogen treatment leads probably to Rhodium diffusion out of titanate lattice, yielding a self-decoration of the nano-sized Barium Titanate particles. Further NO-sensing tests of the sensors produced by deposition of this in-situ Rh-loaded $BaTiO_3$ on the interdigitated electrode (IDE) revealed, for the first time, the achievement of significantly increased selectivity and NO sensing response (~18 % for 200 ppm NO) under a hot-gas environment (synthetic humid air as carrier gas at 900 °C). The calculated response and recovery times are reasonable, and observed reproducibility confirms suitability to practical applications. Relying on the carried investigations, this good sensing performance can be explained by creating excessive oxygen vacancies resulting from rhodium's surface diffusion. Moreover, it is to claim that rhodium's excellent catalytic activity plays a key role in enhancing NO-sensing.

Keywords: Rh-loaded $BaTiO_3$, co-precipitation, high-temperature sensor, nitrogen oxide.

1. Introduction

Nitrogen oxide (NO) is a severely toxic gas with a pungent odor and greenhouse gas contributing to global warming. It arises from nature caused effects (lightning strikes, biological decay, volcanoes, etc.) but increasingly due to the reasons caused by human activities such as combustion of coal and oil at electric power plants, combustion of chemical plant and also in emissions from automotive and aircraft engines. The latter constitutes significantly to the NO sources. NO-emission leads to harmful effects on the environment and health. The environmental effect includes photochemical smog, ozone production, and acid rains. NO can damage the respiratory system and also causes neurodegenerative diseases [1-4]. Even it is complicated to control the NO-emission from the natural effects, it is technically possible to monitor the NO-emission generated from the human activity-related causes). It is to note that the NO produced by human activities involve generally hot gas (> 400 °C) [5,6]. To reduce the

harmful effect of NO on the human environment and health, it is necessary to have a fast and real-time detection system at high temperatures. This detection system is also very important for monitoring the complete combustion of fuel and controlling chemical and metallurgical processes occurring at intermediate-temperatures [7]. Therefore, there is an urgent need to develop sensor control systems for exhaust emission gases to directly monitor NO at temperatures in the range of 400 – 900 °C.

The standard technology used for NO-detection includes bulky and expensive instruments such as optical spectroscopy and gas chromatography. Moreover, their adaption into the high-temperature detection system is complex, costly, and in some cases impossible [8,9]. Besides, the sample preparation is very complicated, and the system does not permit real-time measurement. Chemiresistive gas sensors based on semiconductor metal oxides have been drawing more and more attention because of their advantages such as low cost, lightweight, fast response/recovery times, and high compatibility with microelectronic processing [10,11]. However, most of the simple metal oxides (In_2O_3, Cr_2O_3, Co_3O_4, SnO_2, etc.) display the optimum sensitivity at temperatures below 400 °C [12-15]. Even TiO_2 which is known as a chemically stable metal oxide at high temperature can operate as a gas sensing material at temperatures solely up to a maximum of 800 ºC [16-18]. The stability of a gas sensor based on nanostructured semiconductor oxides at high temperatures can be enhanced by using high stable metal oxide compounds such as barium titanate. Based on the fact that perovskite structured material is also reported to act as a highly stable catalyst at high temperatures (up to 1200 °C and display the flexibility to accommodate dopants, the interest to apply perovskite for high-temperature sensing application is growing [19].

Barium titanate ($BaTiO_3$) is a well-known perovskite material with excellent dielectric, ferroelectric and piezoelectric properties. Besides being an electro-ceramic material necessary in the manufacturing of thermistors, electro-optic devices, and multilayer capacitors, it is also a good photocatalyst [20, 21]. Other ferroelectric materials have been extensively used as gas sensors and showed interesting results [22, 23]. However, there are up-to-date only very few works reporting $BaTiO_3$ sensing properties. Among the studies related to doped barium titanate, Rh-doped $BaTiO_3$ has retained attention because of its appreciable gas sensing properties [24-26]. Its use in a sensor application by Saruhan et al. showed that this material has a high potential for detecting NO_2 at temperatures above 600 °C as a catalytic filter layer on Al-doped TiO_2 and single-layer sensing material [24]. Its chemical stability at high temperatures makes it attractive for high-temperature gas sensor applications. Moreover, nano-sized materials became interesting due to the broader use of miniaturized devices with improved properties.

Despite the high-temperature NO_2-sensing capability achieved with the citrate route synthesized Rh-doped $BaTiO_3$, the work reported by Saruhan et al. revealed that the NO_2-sensitivity of this sensing material was relatively low when another carrier gas such as nitrogen was used, and it was insensitive to detect NO. It is rather challenging to detect NO_2 and/or NO simultaneously and selectively using chemo-resistive gas sensors. This is due to the oppositely occurring oxidizing (NO_2) and reducing (NO) natures of these two gas species. This characteristics gains importance, especially at temperatures above 500 °C since the thermodynamic equilibrium for NO_2/NO in the temperature range of 500 to 800 °C implies both species' presence at the same time in the medium. Thus, as it is reported by Saruhan et al. [18,

24], this phenomenon is the cause of the absence of sensitivity and selectivity of NO-detection above 600 °C. This obstacle can be overcome through material engineering involving nanostructured particle synthesis and segregation of integrated Rh as metallic nano-sides by self-decoration.

In this context, we synthesized Rh-loaded $BaTiO_3$ nanoparticles employing an optimized co-precipitation synthesis route [27] and used these particles for gas sensing. Subsequently, we report, to the best of our knowledge for the first time, excellent NO-sensing performance at 900 °C under humid air achieved by using Rh-loaded $BaTiO_3$ nano particulates as single sensing layers. For that, we employed an oxalate-assisted co-precipitation synthesis route [27] and a post thermal hydrogen treatment to yield the desired in-situ decoration of $BaTiO_3$ with Rh-NPs. The exhaustive material characterizations revealed the possibility that Rh diffuses out of the $BaTiO_3$ lattice under a reducing environment of the thermal hydrogen treatment to decorate the surface of perovskites in-situ with extremely small Rh-NPs yielding the selective detection of NO in the hot synthetic air environment (900 °C). These results are being reported for the first time.

2. Materials and methods

2.1 Materials

Barium acetate ($Ba(C_2H_3O_2)_2$, 98% Chempur), Titanium isopropoxide ($Ti\{OCH(CH_3)_2\}_4$, 99.999% Aldrich), and Rhodium nitrate ($Rh(H_2O)(OH)_{3-y}(NO_3)y$ y=2-3, 15.19 % Chempur), oxalic acid ($C_2H_2O_4.2H_2O$, 99.5% Chempur), Acetic acid (99.9 %, Chemsolute) and absolute Ethanol (Chemsolute) are used in the forms as received from suppliers without further purification or processing.

2.2 Preparation of powder samples

The synthesis of Rh-doped $BaTiO_3$ (designated as BTR1-OX-900) was followed over two steps as previously reported in the literature [27]: (*i*) the first step involved the preparation of a precursor solution containing barium, titanium, and rhodium ions in the right ratio in accordance with the given chemical formula. Barium acetate was dissolved in acetic acid, titanium isopropoxide, and rhodium nitrate were diluted separately by adding pure ethanol. All the prepared solutions were mixed and stirred for 5 min to obtain a yellowish solution. The amount of the aqueous Rh-nitrate solution was adjusted to yield perovskites with the following composition: $BaTi_{0.98}Rh_{0.02}O_3$. (*ii*) In the second step, this precursor solution was then co-precipitated using an oxalate ligand as a precipitating agent, which was subsequently decomposed by heating. To prepare the oxalate ligand, oxalic acid was dissolved in ethanol solution and poured progressively in the previously prepared (metal) cationic precursor. The resulting mixture was stirred for one hour to allow complete precipitation. The so-obtained precipitate was filtered and dried in an oven at 80 °C yielding a yellowish powder. The as-prepared precursor powder was calcined in a ceramic combustion boat holder at 900 °C in a muffle furnace (5 °C min^{-1}) for one hour under static air.

2.3 Preparation of sensor

For gas-sensing measurements, the as-prepared Rh-doped $BaTiO_3$ powders were deposited as thick films on alumina substrates that were previously fitted with interdigitated Pt – electrodes (IDE), using a simple drop-coating of the corresponding ink. The interdigital design consisted of 10 interdigital bars of 300 µm wide and 2 mm long that had a gap of 300 µm between each other. The ink was prepared by mixing the metal oxide powder ground with agate mortar with distilled water. After the deposition, the sensing layer (~20 µm) was activated by a heat treatment under 2 % of hydrogen at 900 °C for 1h leading to the formation of Rh-loaded $BaTiO_3$.

2.4 Characterization

The XRD diffractograms of all the samples were obtained at room temperature with a D5000 Siemens Kristalloflex Θ-2Θ powder diffractometer which has a Bragg-Brentano geometry and equipped with Cu-Kα radiation (λ= 1.54178 Å) and a standard scintillation counter detector. For the experiment, the as-prepared material was pressed in the sample holder and the patterns were recorded in the range of 5-80° with a scan step of 0.02 (2Θ) and a 2 s $step^{-1}$. The program EVA from BRUKER AXS was used to assign the reflexes to the experimental diffractogram from the JCPDS (Joint Committee on Powder Diffraction Standards) database.

Bruker Senterra Raman spectrometer (from Bruker Optik GmbH, Ettlingen, Germany) was used to record all the Raman spectra at room temperature under 532 nm and 0.2 mW power laser excitation, which was focused on samples through a 50X objective (Olympus MPlan N 50X/0.75).

The elemental composition and the chemical state of the various constituents of all the synthesized samples were done by X-ray photoelectron spectroscopy (XPS) measurements. It was performed using an ESCA M-Probe Spectrometer from Surface Science Instruments, equipped with a monochromatic Al Kα excitation source (λ = 8.33 Å), at a pressure in the range of 10^{-8} to 10^{-9} mbar. Survey and high-resolution scans were performed with a detector pass energy of 158.9 eV and 22.9 eV, respectively. All spectra were referenced to the adventitious carbon signal at 284.8 eV. Curve fitting was performed using a Gaussian-Lorentzian peak shape after performing a Shirley background correction. Additionally, a DS (0.0001,400) line shape was used to fit the elemental rhodium peaks. Spectral corrections and peak fitting were done with Casa XPS software (Casa Software Ltd.).

The particles' morphology was determined by Scanning Electron Microscopic (SEM) analysis and was carried out in a Zeiss Ultra 55 microscope equipped with an Energy Dispersive X-ray Spectrometer (EDS) from Oxford Instruments. Before the analysis, the samples were sputtered with Platine particles to avoid the charge effect.

2.5 Gas sensing measurement

Measurement of the sensors' electrical resistance changes in the presence of the target gases was carried out in a specially constructed apparatus consisting of a tube furnace with cascade control and a custom-built quartz glass reactor providing a thermocouple directed at the specimen. The mixed gas composition was controlled by a six-channel mass flow controller (MFC-647b from M composition KS Instruments GmbH). The gas flow rate was adjusted to

400 mL/min, and the NO concentrations were varied between 50 and 200 ppm. Mostly dry or humid synthetic air (80% N_2 + 20% O_2) was used as the carrier gas. The moist air was obtained by humidification at 50 °C of dry air through a water bubbler. The DC electrical measurements were carried out using a Keithley 2635A source meter with a computer-controlled LabView program. After the sensors' electrical resistance was stable in reference atmosphere air (R_{air}) and then waiting for another 10 min, the desired amount of NO was introduced into the chamber for 10 min. R_{gas} is obtained until the sensor resistance is stable in the presence of the target gas. The sensor response (S) of Rh doped $BaTiO_3$, which behaves as a p-type semiconductor, is defined by $(R_{air}/R_{gas} - 1) \times 100$ and $(R_{gas}/R_{air} - 1) \times 100$ for oxidizing and reducing gases, respectively. These measurements were carried out at different operating temperatures ranging from 600 to 900 °C.

3. Results and Discussion

The results of XRD analysis performed on the sample powders (designated as BTR1-OX-900) before and after the heat treatment under hydrogen are presented in Figure 1a. As shown, both powders display $BaTiO_3$ (according to JCPDS 075-0462) as a major phase and a trace amount of $BaCO_3$ phase. However, after H_2 treatment, a decrease in the intensities of $BaTiO_3$ peaks is observed (for example, at two thetas = 31.2 °) while the $BaCO_3$ peaks remain unchanged (for example, at two thetas = 24 °) as depicted in Figure 1.b. This decrease at the $BaTiO_3$ peaks can be assigned to a decrease in its crystallinity. In fact, before the H_2-treatment (Rh-doped $BaTiO_3$), Ti^{4+} is substituted by Rh^{3+} as reported in our previous work.[27] After the H_2 heat treatment (Rh-loaded BaTiO3), Rhodium ions probably undergo a reduction and moves outside of the $BaTiO_3$ structure, disturbing, therefore, its structural order, resulting in reduced crystallinity and, in turn, the decrease in the intensities of the peaks. The absence of a Rhodium-containing phase in this sample could be due to the small quantity (0.4 at %) and the Rhodium's well dispersion on the $BaTiO_3$ particle surfaces. The absence of such a phase indicates probably that there is almost no agglomeration of Rhodium on the $BaTiO_3$ surfaces after H_2 heat treatment, which can be of great benefit for sensing application. This behavior of Rh-doped $BaTiO_3$ is similar to what has been already reported in the literature concerning Rh-doped $CaTiO_3$ which is structurally very similar to the Rh-doped $BaTiO_3$ [28].

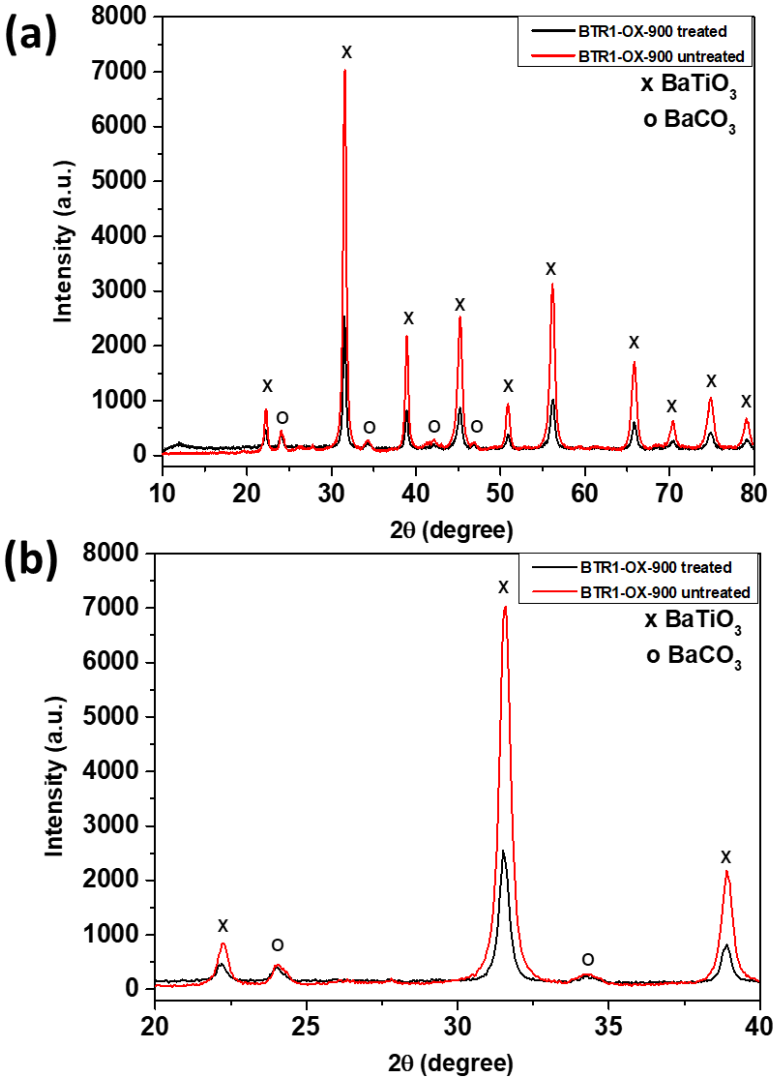

Figure 1. (a) Powder XRD patterns of untreated and hydrogen treated BTR1-OX-900, (b) Zoom of the most intense peaks.

Raman spectra of both as-prepared and hydrogen heat-treated Rh-doped $BaTiO_3$ are displayed in Figure 2. These two spectra show almost the same peaks with the ones observed at 270, 308, 525, and 725 cm^{-1} which are assigned respectively to the A1(TO2), E(TO2), A1(TO3), and A1(LO3) of barium titanate modes of the room temperature P4mm phase [29]. However, a significant decrease in the peak intensities can be observed after hydrogen treatment. This indicates an increase of disorder in the barium titanate lattice since Raman scattering spectra are more sensitive to short-range ordering structure. In fact, after heat treatment, the Rhodium ions are reduced to metal and probably diffuses outside the $BaTiO_3$ structure, and this could result in the creation of defects such as oxygen vacancies in Barium Titanate lattice to compensate the charge and, therefore, disturb the structural order of $BaTiO_3$. A similar observation has already been reported in the literature [30]. This result corroborates well with what has been obtained in XRD. The increasing number of oxygen vacancies can play a significant role in the enhancement of sensing properties.

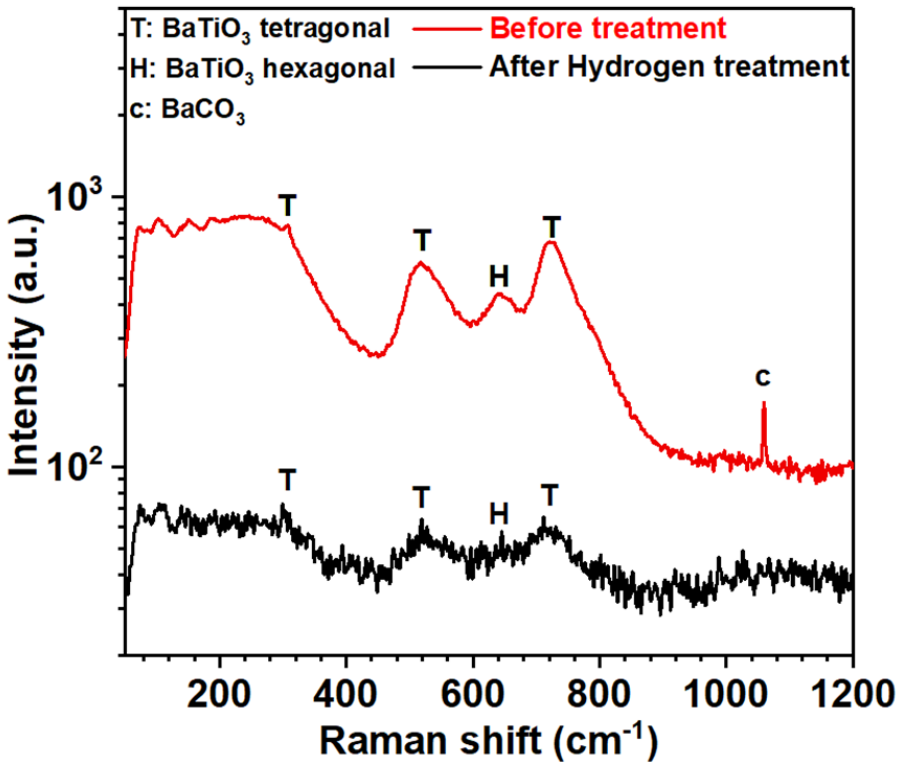

Figure 2. Raman spectra of untreated and hydrogen treated Rh-doped $BaTiO_3$.

The chemical states and the composition of the as-prepared and hydrogen-treated sample powder were investigated by XPS analysis. As revealed in Figure 3, both samples are composed of barium, titanium, rhodium, oxygen, and carbon. As far as the chemical states of the constituents are concerned, the high-resolution XPS spectra (Figure 4a) showed the presence of Ba3d5/2 line in the two samples represented by duplets at 778.23, 793.56 eV and 777.79, 793.12 eV for untreated and hydrogen treated samples, respectively. These values correspond to the binding energies of Ba3d of $BaTiO_3$ and agree with those reported in the literature [31]. A slight difference of 0.44 eV observed between these binding energies can be due to the chemical environment's difference resulting in the change of oxidation state of the rhodium. After deconvolution, an additional duplet of Ba3d peak is observed at 779.60, 794.93 eV, which can be assigned to a small amount of $BaCO_3$ also observed in XRD analysis [32]. The energies of the Ti2p3/2 lines in the high-resolution XPS spectra are centered around 457.60, 463.32 eV, and 457.20, 462.92 eV for the untreated and hydrogen treated samples, respectively (Figure 4b). These binding energies can be assigned to Ti^{4+} in $BaTiO_3$, as reported in the literature [31]. A second duplet appears in the Ti 2p at 458.94, 464.66 eV and 458.95, 464.67 eV and can be assigned to TiO_2 [33]. This phase could be in trace amount since XRD and Raman analyses did not reveal it. A small difference of 0.40 eV between these values is also observed. Concerning the rhodium (Figure 4c), the lines for Rh3d 5/2 observed in an untreated sample at 309.43, 314.14 eV can be attributed to Rh^{3+}, suggesting the substitution of Ti^{4+} by Rh^{3+} in $BaTiO_3$ structure. However, after hydrogen treatment, shifting to lower binding energies (306.59, 311.30 eV) of this previous line is observed, which can be attributed to the metallic Rhodium. This confirms definitely the fact that the hydrogen treatment provokes the reduction of Rhodium and probably its migration from the inside (Rh^{3+}) to outside (Rh^0) of the structure. Thus, we obtained a kind of self-decoration of $BaTiO_3$ by metallic Rhodium. There is obviously

a shift to lower binding energies for these peak sets, Ba3d (from 778.23, 793.56 eV to 777.79, 793.12 eV) and Ti 2p (from 457.60, 463.32 eV to 457.20, 462.92 eV). This suggests the presence of defects that change the chemical environment inside the $BaTiO_3$ due certainly to the reduction and probably the migration of rhodium outside the structure. In fact, to compensate for the charge difference after reducing rhodium, oxygen vacancies can be created.

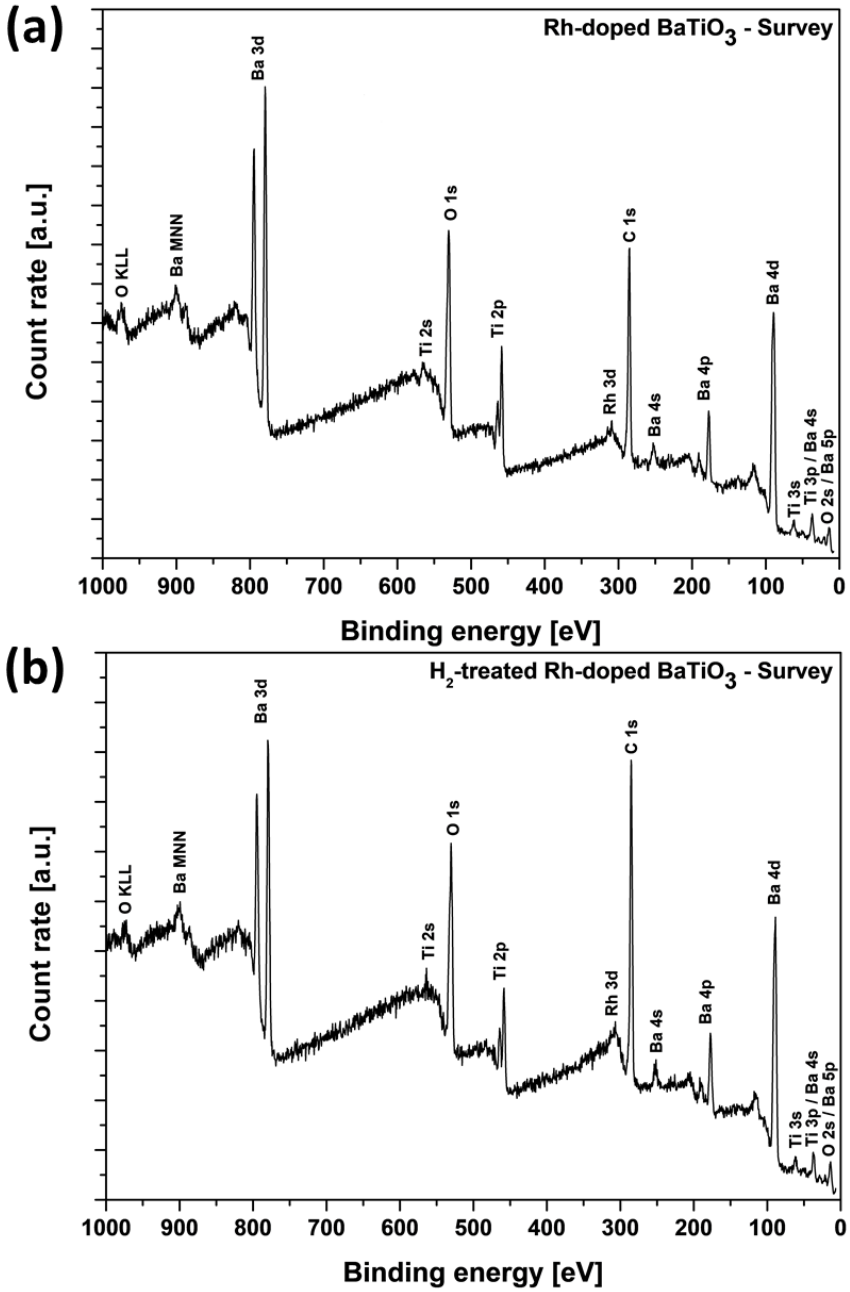

Figure 3. XPS survey spectra of (a) untreated Rh-doped $BaTiO_3$ and (b) hydrogen treated Rh-doped $BaTiO_3$

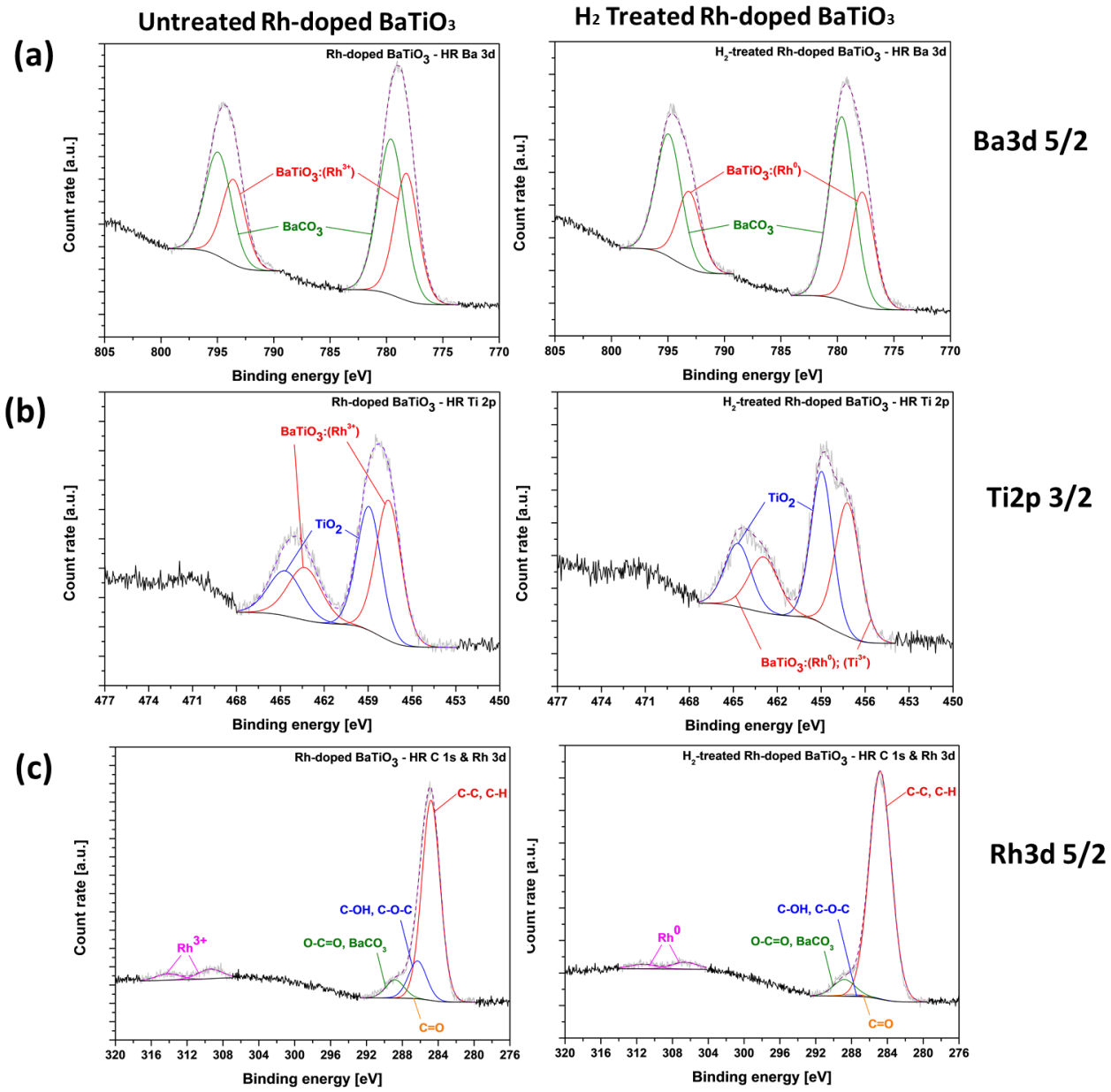

Figure 4. The high-resolution XPS survey spectra of the untreated and hydrogen treated Rh-doped $BaTiO_3$ (a) Ba3d 5/2, (b) Ti2p 3/2, (c) Rh3d 5/2.

The morphologies of the particles obtained before and after H_2 treatment are shown in Figure 5. As it is clear, already at first glance, the hydrogen heat treatment does not significantly influence the morphology of $BaTiO_3$-nanoparticles. As shown in SEM pictures, this oxalate co-precipitation route enables the achievement of the well-defined and homogeneously distributed spherical nanoparticles (~50 nm). It can also be remarked that there are very little agglomeration and extremely low sintering of particles which was not the case when the classic route was used for the synthesis [27]. In fact, the oxalate ligand's presence avoids the particles' stacking by steric hindrance during decomposition. Thus, the individual growth of Rh-doped $BaTiO_3$ is promoted. This type of morphology with less agglomeration can be a benefit for sensing applications. Since the particles obtained with oxalate co-precipitation route are really fine and the amount of rhodium is exceptionally low (0.4 at %), it was difficult to observe the metallic

rhodium precipitate on the surface of perovskite after H_2 treatment comparing to the observations given in Saruhan et al. where the classic route was used to prepare large and prismatic shaped grains of Rh-doped $BaTiO_3$ particles (1 at % of Rh) [24].

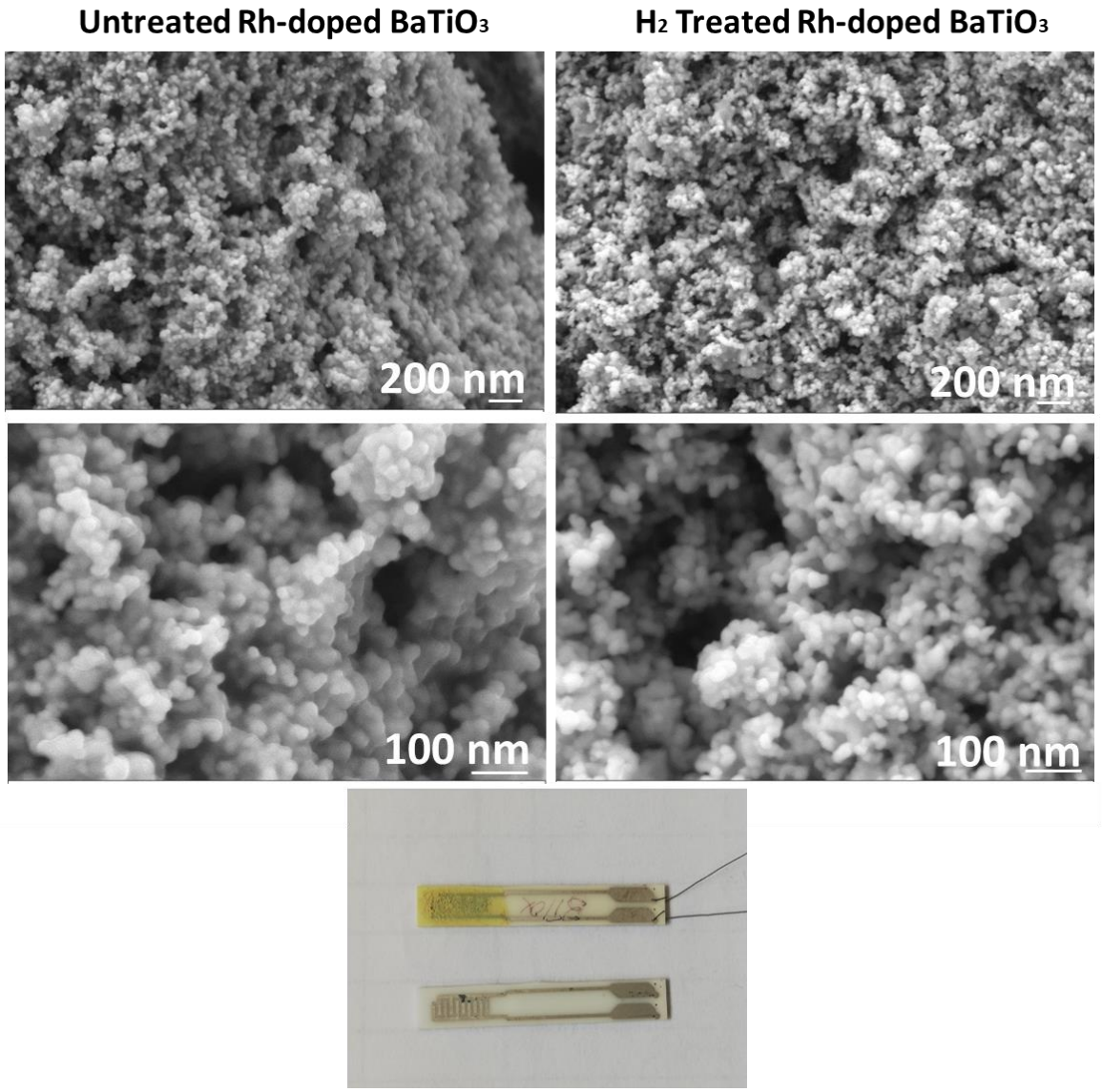

Figure 5. Sensor photograph and SEM images of untreated and hydrogen treated Rh-doped $BaTiO_3$ at different magnifications.

As humidity is always present in the exhaust gas stream, all the gas sensor tests that have been performed in humid air (10 % of relative humidity, RH) are presented here. The temperature is among the key parameters influencing the sensing response of a gas sensor. Figure 6 a and b show the sensor responses of the hydrogen treated Rh-doped $BaTiO_3$ towards 200 ppm of nitrogen oxide (NO) at a different operating temperature under dry and humid synthetic air and the dynamic response at 700 and 900 °C, respectively. The sensor responses are 14, 2, 6, 7 % in dry air, 6, 12, 16, and 18 % in humid air at 600, 700, 800, and 900 °C, respectively. In dry air, the sensor response decreases from 14 to 7 % in general with the increasing temperature,

while in humid air, the sensor response increases from 6 to 18 % as the temperature increases. The maximum sensor response is therefore obtained at 900 °C under humidity. This enhancement of sensing properties in the presence of humidity can be explained by the affinity between adsorbed hydroxyl group (generated after thermal decomposition of water) and the NO. In fact, at high temperatures, H_2O in water vapor decomposes, and hydroxyl is adsorbed on the sensing layer. As the temperature increases, more decomposition will occur, and more hydroxyl groups will be adsorbed on the surface, enhancing the NO sensor response. It is the first time that NO is detected at such a high temperature in the humid air, to the best of our knowledge. We have therefore decided to investigate other sensing properties of this material at 900 °C under humid air.

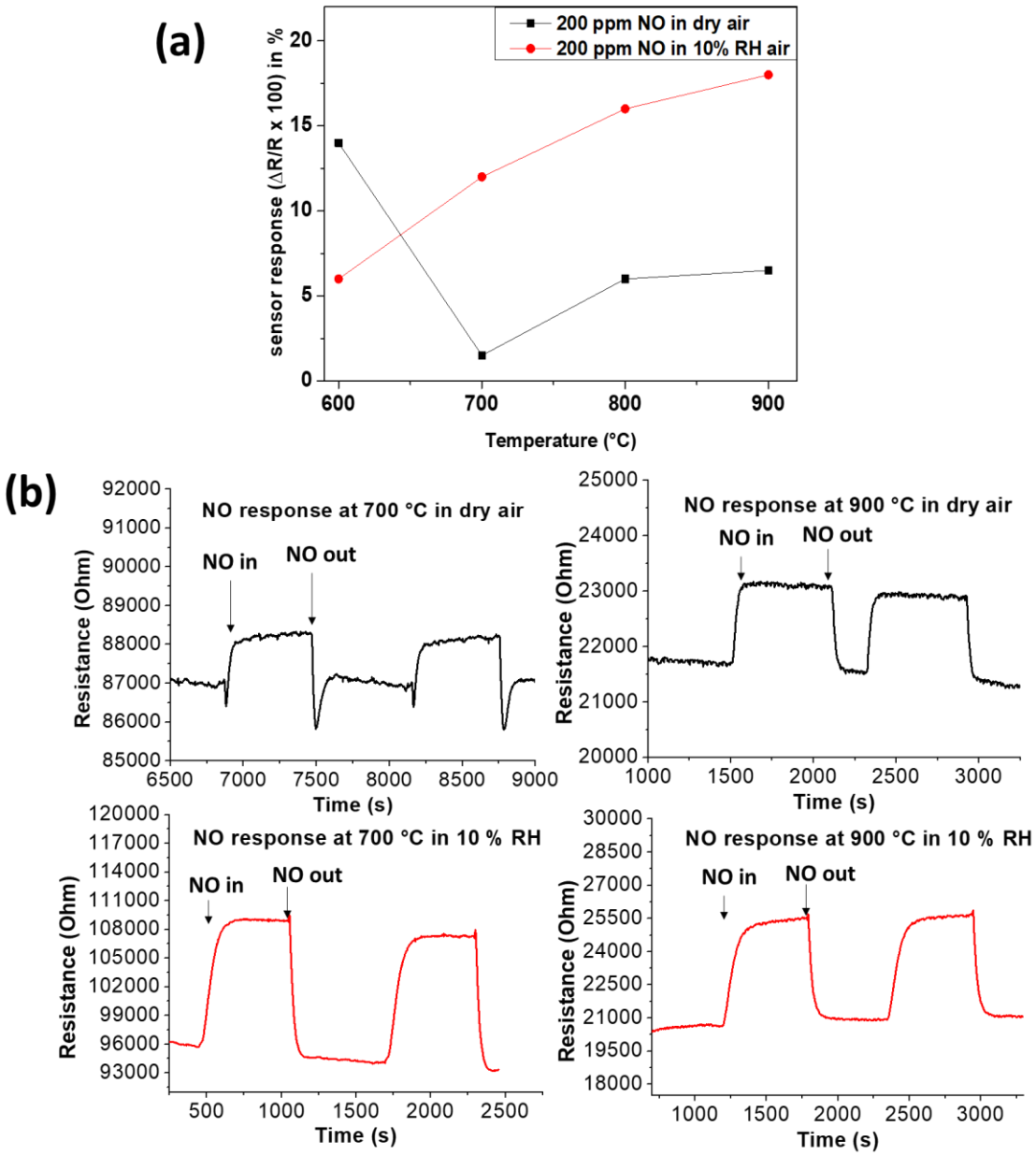

Figure 6. (a) Response of gas sensor based on hydrogen treated Rh-doped $BaTiO_3$ to 200 ppm of NO in dry and humid air (set at 50 °C) at different operating temperatures and (b) the corresponding dynamic response at 700 and 900 °C

To evaluate the sensor's possibility to be used for quantitative analysis, the sensor responses at different NO concentrations in humid air have been measured in a specific order and randomly. As observed in Figures. 7a and 7b, the responses obtained are 5, 8, and 18 % for 50, 100, and 200 ppm NO, respectively. It can be remarked that the sensor response increases with the increasing NO concentrations, indicating that the sensor can be used to quantify the amount of NO in the exhaust gas stream, which is very important for practical applications. Moreover, it is observed that the change of the sensor response is proportional to the NO concentration when NO concentration during the test is randomly changed (Figure 7b).

The reproducibility of a gas sensor is also a very important characteristic. The sensing responses have been measured after introducing 200 ppm NO successively four times under the same conditions. As it can be observed in Figure 7c, for all four cycles, the sensor resistance increases until the sensor stability is reached when NO is injected, and when the test gas is vented, the resistance returns almost to its initial value. Even though a negligible drift is observed, the sensor displays good reproducibility. Real-time gas detection is one of the advantages of resistive gas sensors. The response and the recovery times have been also evaluated by measuring for 200 ppm of NO, the time required by the sensor to reach 90 % of its steady-state gain value after the introduction of target gas, and the time took by the sensor to be within 10 % of the value as it had before its exposure to target gas, respectively. The response and recovery times are calculated to be 160 s (2.6 min) and 64 s (1.1 min), respectively. Even though these values are higher than those usually found in the literature for this type of sensor [10], the response and recovery times exhibited by our sensor are reasonably good for practical application and far better compared to the traditional type of sensor [8,9].

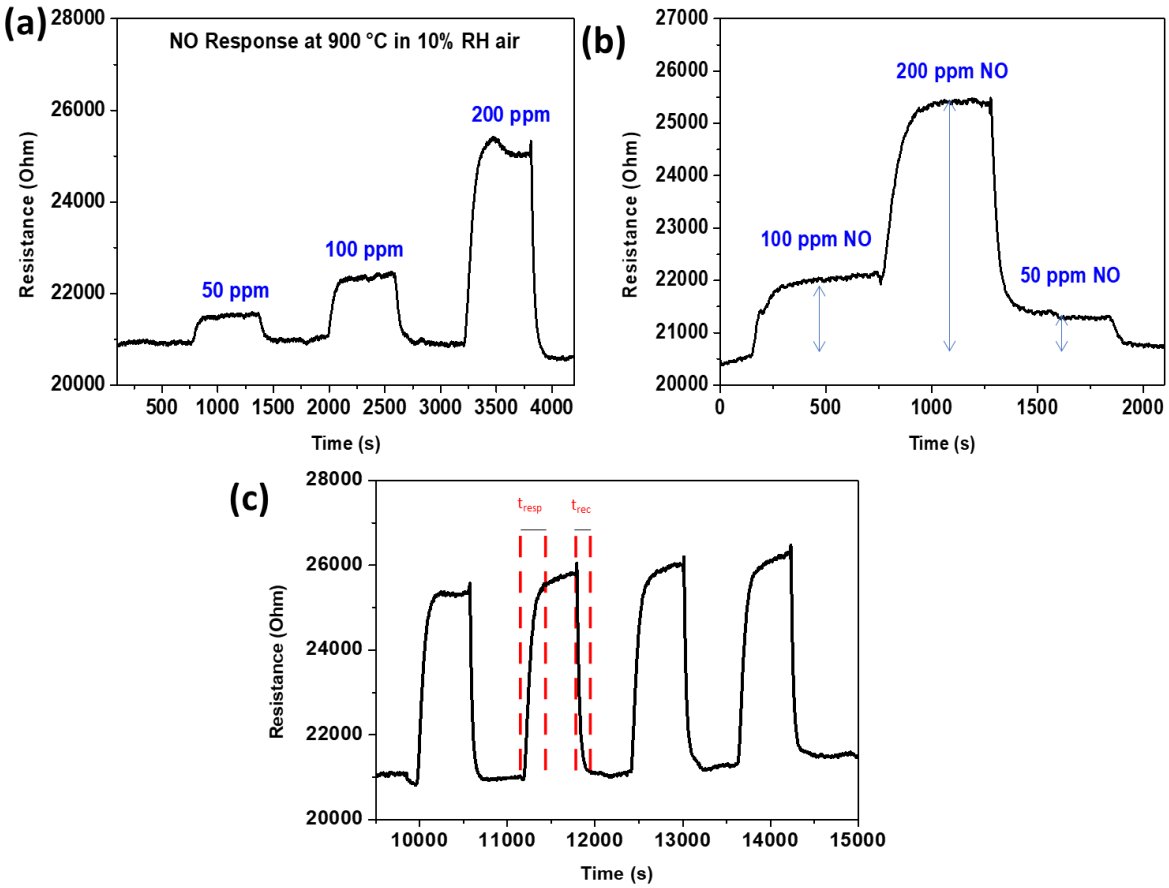

Figure 7. Dynamic response of gas sensors based on hydrogen treated Rh-doped $BaTiO_3$ in humid air (set at 50 °C) to (a) various concentrations of NO injected in order, (b) various concentrations of NO injected randomly, and (c) 200 ppm NO at 900 °C.

Two other main products for fuel combustion are NO_2 and CO. Their presence in the exhaust gas stream at a high temperature can cause important hinders for the NO gas sensing application. Our sensor's selectivity toward NO against CO and NO_2 at 900 °C under humid air was investigated. Figure 8 shows the different responses of the sensor to 200 ppm of NO, NO_2 and CO. The results indicate that at 900 °C, the response to 200 ppm of NO (18 %) is higher than that of 200 ppm of NO_2 (8.7 %) and 200 ppm of CO (8.4 %). This implies that this sensor is at least twice more sensitive to NO than NO_2 and CO. This good selectivity is ascribed to the catalytic effect of Rhodium-NPs on the oxidation of NO, which will promote and enhance the adsorption and the oxidation of NO preferentially. It is reported in the literature that Rhodium which is currently and often used in TWC, is a suitable catalyst for NO oxidation [34].

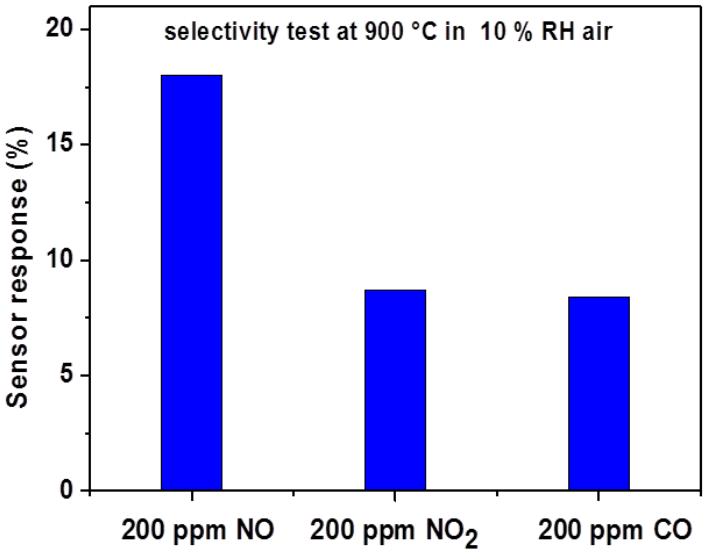

Figure 8. The response of gas sensor based on hydrogen treated Rh-doped $BaTiO_3$ to various gases including 200 ppm of NO, NO_2, and CO all in humid air (set at 50 °C) at 900 °C.

Since the exhaust combustion gases always contain humidity, the humidity effects on NO sensor responses have been investigated. The dynamic responses to 200 ppm of NO at different humidity levels (10, 7.5, 5, 2.5, and 0 %) have been recorded at 900 °C in air and the results are presented in Figure 9. As can be observed, the NO sensor response decreases gradually with the decrease of humidity level. The observed decrease of NO sensitivity can be ascribed to the achievement of high affinity between –OH species and NO. In the presence of humidity, water molecules will be decomposed, and the hydroxyl group adsorbed on the perovskite surface; NO will therefore be readily adsorbed by means of the Van der Waal forces between O-H and NO. This will lead to the enhancement of NO-adsorption when the humidity increases. When the humidity level decreases, there is less hydroxyl group adsorbed on the surface and less NO, decreasing the NO sensor response.

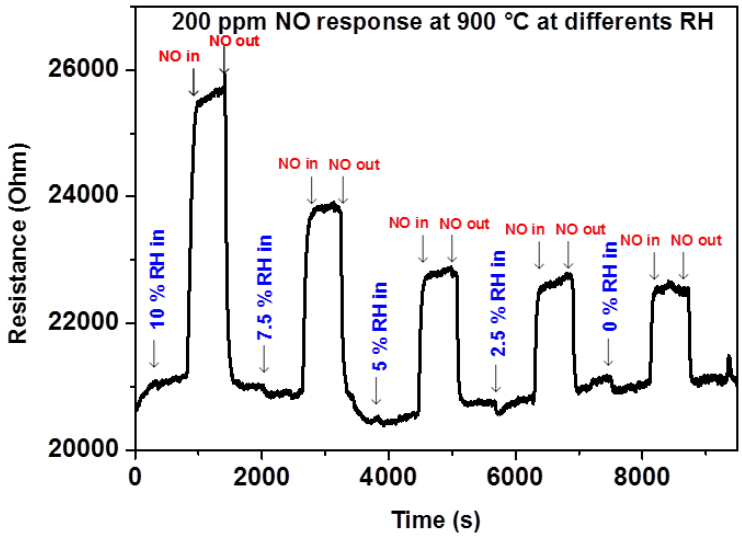

Figure 9. Dynamic response of gas sensors based on hydrogen treated Rh-doped $BaTiO_3$ to 200 ppm of NO at 900 °C in different relative humidity percentages set at 50 °C (10, 7.5, 5, 2.5, and 0 % of RH).

Table 1 highlights a comparison between the optimum sensing temperature achieved in the present sensor and the other high-temperature sensors, which were reported in the previous literature. Although the measurement methods at the laboratories of the previous work differ and thus lead to the differences in response type, Table 1 evidently shows that the present sensor operates well at the highest temperature of 900 °C and is superior to most of those reported as high-temperature capable NO-sensors.

Table 1: Comparison of the optimum sensing temperature of the present sensor and that of devices reported previously in the literature.

Materials	Sensor type	NO concentration (ppm)	Working Temperature (°C)	Response	Ref
Cr_2O_3	Mixed-potential	500	475	-29.27mV	[35]
$NiCr_2O_4$	Mixed-potential	200	650	-25 mV	[36]
$ZnFe_2O_4$	Mixed-potential	200	700	-7 mV	[37]
ZnO	Mixed-potential	200	700	-17 mV	[38]
Pt-WO_3/TiO_2	impedancemetric	400	500	71 %	[39]
Pt-$SrSnO_3$-WO_3	capacitive	100	550	1.5	[40]
Bi_2MoO_6	resistive	20	300	3.13	[41]
$ZnGa_2O_4$	resistive	6.25	300	22.21	[42]
Rh-doped $BaTiO_3$	resistive	200	900	18 %	**This work**

Sensing mechanism

Rh-doped $BaTiO_3$ is a p-type semiconductor, and its gas detection principle is based on the change of electrical resistance in the presence of target gas. As all the resistive gas sensors, in synthetic air, the oxygen molecules are readily adsorbed on the sensing layer's surface and get ionized (O_2^-, O^-, O^{2-}) by taking electrons from the conduction band. At high temperature (above 300 °C), O^{2-} is the dominant species. This creates a hole accumulation layer and a decrease in electrical resistance. On injection of NO, after its adsorption on sensing layer, an oxidation reaction with the ionized oxygen will take place (eq.1), and the released electrons will return to the conduction band filling the holes leading to the increase of sensor resistance, as a result of thinning of the hole accumulation layer. In our case, the sensing layer's hydrogen treatment at an elevated temperature enhances the sensing properties considerably. In fact, the hydrogen treatment provokes the reduction and probably the diffusion of Rhodium from inside to outside of $BaTiO_3$ lattice, generating more oxygen vacancies and by creating a kind of metallic Rhodium self-decoration of $BaTiO_3$ where Rh acts as a well-known catalyst. Besides, the increase of oxygen vacancies narrows the bandgap width of semiconductors, increases the

active sites on the material surface, and enhances the chemisorption, thus improving the material's adsorption performance and consequently the sensing response [43]. On another side, the enhancement of chemical and electronic sensitization may happen with the presence of well-dispersed Rh metallic nanoparticles on the $BaTiO_3$ surface. The Rh's potential to attract more O_2 molecules to adsorb on the surface will lead to chemical sensitization [44]. As more oxygen is adsorbed on the surfaces, more reaction between ionized oxygen and NO will lead to an enhanced sensor response. The electronic sensitization may also be induced by the metallic Rhodium decoration of $BaTiO_3$ nanoparticles, because of the Rhodium's work functions (4.97 eV), which are higher than that of $BaTiO_3$ (4.54 eV). This might result in energy band bending at the Rh/$BaTiO_3$ interface. The formation of an additional depletion region at the Rh/$BaTiO_3$ interface is favored by the Schottky contacts between the $BaTiO_3$ and Rh nanoparticles. This would lead to greater change in the baseline resistance resulting in a huge variation in resistance in the presence of NO gas. Moreover, the metallic Rhodium decorating the surface yields a good catalyst for NO oxidation and will therefore enhance preferentially the adsorption and oxidation of NO, increasing the sensor's selectivity toward NO [34]. The enhancement of sensitivity also observed under humid air is due to the increase of NO adsorption due to the hydroxyl groups' presence (coming from the decomposition of water molecules before reaching the surface) which have a high affinity with NO because of the hydrogen bonds between the two species. A similar effect of water has been reported in the literature [45-47].

$$NO_{(gas)} + O_{ads}^{2-} \rightarrow NO_{2(gas)} + 2e^{-} \quad (1)$$

4. Conclusions

Rh-doped $BaTiO_3$ nanoparticles have been prepared by oxalate co-precipitation route and activated further by heat treatment under hydrogen at 900 °C for sensor application, yielding improved NO-sensing properties. The material characterization results by XRD, Raman, and XPS indicate the substitution of Ti^{4+} by Rh^{3+} in Barium Titanate structure before the hydrogen treatment and the self-decoration of that structure by metallic Rhodium after hydrogen treatment due certainly to the diffusion of Rhodium from lattice inside to outside in reducing environment. The nanoparticles of Rh-doped $BaTiO_3$, free of any sintering, have been tested as a NO gas sensor under synthetic humid air at high temperatures (900 °C). For the first time, it was possible to detect NO at 900 °C under humid air with a good response (18 % for 200 NO ppm), good selectivity (twice more sensitive to NO than CO and NO_2), and reasonable stability, response, and recovery times. The enhancement of sensing properties observed is due to Rhodium diffusion outside the $BaTiO_3$-lattice, which creates more oxygen vacancies and also to adsorption of the hydroxyl group on the surface. The catalytic activity of metallic Rhodium is also a crucial factor. This work opens a new perspective in the synthesis and use of doped complex metal oxides for high-temperature NO-detection.

Acknowledgment

The grant provided by the DLR-DAAD Fellowship program under no. 284 is acknowledged

5. References

[1] T. Boningari, P. G. Smirniotis, Impact of nitrogen oxides on the environment and human health: Mn-based materials for the NOx abatement. Curr Opin Chem Eng. 13 (2016) 133–141.

[2] F. Gholami, M. Tomas, Z. Gholami, M. Vakili, Technologies for the nitrogen oxides reduction from flue gas: A review. Sci. Total Environ. 714 (2020) 136712.

[3] I.A. Resitoglu, NOx Pollutants from Diesel Vehicles and Trends in the Control Technologies. IntechOpen (2018). doi 10.5772/intechopen.81112.

[4] F. Gao, X. Tang, H. Yi, S. Zhao, C. Li, J. Li, Y. Shi, X. Meng, A review on selective catalytic reduction of NOx by NH_3 over Mn–based catalysts at low temperatures: catalysts, mechanisms, kinetics and DFT calculations. Catalysts 7 (2017) 199.

[5] İ. A. Reşitoğlu, K. Altinişik, A. Keskin The pollutant emissions from diesel-engine vehicles and exhaust aftertreatment systems. Clean Technol Environ Policy 17 (2015) 15–27.

[6] J. Yanik, G. Duman, O. Karlström, A. Brink, NO and SO_2 emissions from combustion of raw and torrefied biomasses and their blends with lignite. J. Environ. Manage. 227 (2018) 155-161.

[7] N. Docquier, S. Candel, Combustion control and sensors: a review. Prog. Energy Combust. Sci. 28 (2002) 107-150.

[8] L. B. Kreuzer, C. K. N. Patel, Nitric Oxide Air Pollution: Detection by Optoacoustic Spectroscopy. Science 173 (1971) 45-47.

[9] P. J. Kipping, P. G. Jeffery, Detection of Nitric Oxide by Gas-chromatography. Nature 200 (1963) 1314.

[10] D. Nunes, A. Pimentel, A. Gonçalves, S. Pereira, R. Branquinho, P. Barquinha, E. Fortunato, R. Martins, Metal oxide nanostructures for sensor applications. Semicond. Sci. Technol. 34 (2019) 043001.

[11] N. Nasiri, C. Clarke, Nanostructured Chemiresistive Gas Sensors for Medical Applications. Sensors 19 (2019) 462.

[12] S. Roso, D. Degler, E. Llobet, N. Barsan, A. Urakawa, Temperature-Dependent NO_2 Sensing Mechanisms over Indium Oxide. ACS Sens. 2 (2017) 1272-1277.

[13] H. Jin, Y. Huang, J. Jian, Plate-like Cr_2O_3 for highly selective sensing of nitric oxide. Sens. Actuators B Chem. 206 (2015) 107-110.

[14] J. Cao, S. Wang, J. Li, Y. Xing, X. Zhao, D. Li, Porous nanosheets assembled Co_3O_4 hierarchical architectures for enhanced BTX (Benzene, Toluene and Xylene) gas detection. Sens. Actuators B Chem. 315 (2020) 128120.

[15] Y.-X. Li, Z. GuO, Y. Su, X.-B. Jin, X.-H. Tang, J.-R. Huang, X.-J. Huang, M.-Q. Li, J.-H. Liu, Hierarchical Morphology-Dependent Gas-Sensing Performances of Three-Dimensional SnO_2 Nanostructures. ACS Sensors 2 (2017) 102-110.

[16] L. Xie, Z. Li, L. Sun, B. Dong, Q. Fatima, Z. Wang, Zh. Yao, A A. Haidry, Sol-gel Synthesis of TiO_2 with p-Type Response to Hydrogen Gas at Elevated Temperature. Front. Mater. 6 (2019) 96.

[17] Y. X. Liu, J. Parisi, X. C. Sun, Y. Lei, Solid-state gas sensors for high temperature applications–a review. J. Mater. Chem. A. 2 (2014) 9919–9943.

[18] B. Saruhan, A. Yüce, Y. Gönüllü, K. Kelm, Effect of Al doping on NO_2 gas sensing of TiO_2 at elevated temperatures. Sens. Actuators B Chem 187 (2013) 586-597.

[19] K. Simmance, D. Thompsett, W. Wang, B. Thiebaut, Evaluation of perovskite catalysts prepared by flame spray pyrolysis for three-way catalyst activity under simulated gasoline exhaust feeds. Catal. Today 320 (2019**)** 40-50.

[20] M.K. Rath, G.K. Pradhan, B. Pandey, H.C. Verma, B.K. Roul, S. Anand, Synthesis, characterization and dielectric properties of europium-doped barium titanate nanopowders, Mater. Lett. 62 (2008) 2136-2139.

[21] S. Kappadan, T. W. Gebreab, S. Thomas, N. Kalarikkal, Tetragonal $BaTiO_3$ nanoparticles: An efficient photocatalyst for the degradation of organic pollutants, Mater. Sci. Semicond. Process. 51 (2016) 42-47.

[22] K. Mistewicz, M. Nowak, D. Stroz, A. Guiseppi-Elie, Ferroelectric SbSI nanowires for ammonia detection at a low temperature, Talanta 189 (2018) 225-232.

[23] K. Mistewicz, Recent Advances in Ferroelectric Nanosensors: Toward Sensitive Detection of Gas, Mechanothermal Signals and Radiation, J. Nanomater.2018 (2018) 2651056.

[24] B. Saruhan, A. A. Haidry, A. Yüce, E. Ciftyürek, G. C. Mondragón Rodríguez, A Double Layer Sensing Electrode "$BaTi_{(1-X)}RhxO_3$/Al-Doped TiO_2" for NO_2 Detection above 600 °C, Chemosensors 4 (**2016)** 1-16.

[25] A. Petris, M.J. Damzen, V.I. Vlad, Enhanced wave mixing in photorefractive rhodium-doped barium titanate crystals, Opt. Commun. 176 (2000) 223–229.

[26] S. Nishioka, K. Maeda, Hydrothermal synthesis of rhodium-doped barium titanate nanocrystals for enhanced photocatalytic hydrogen evolution under visible light, RSC Adv. 5 (2015) 100123–100128.

[27] R. Lontio Fomekong, S. You, F. Enrichi, A. Vomiero, B. Saruhan, Impact of Oxalate Ligand in Co-Precipitation Route on Morphological Properties and Phase Constitution of Undoped and Rh-Doped $BaTiO_3$ Nanoparticles. Nanomaterials 9 (2019) 1697.

[28] S. Dai, S. Zhang, M. B. Katz, G. W. Graham, X. Pan, In Situ Observation of Rh-$CaTiO_3$ Catalysts during Reduction and Oxidation Treatments by Transmission Electron Microscopy. ACS Catal. 7 (2017) 1579-1582.

[29] H. Hayashi, T. Nakamura, T. Ebina, In-situ Raman spectroscopy of $BaTiO_3$ particles for tetragonal–cubic transformation. J. Phys. Chem. Solids 74 (2013) 957–962.

[30] L. Padilla-Campos, D.E. Diaz-Droguett, R. Lavín, S. Fuentes, Synthesis and structural analysis of Co-doped $BaTiO_3$. J. Mol. Struct. 1099 (2015) 502-509.

[31] C. Miot, E. Husson, C. Proust, R. Erre, J. P. Coutures, Residual Carbon Evolution in $BaTiO_3$ Ceramics Studied by XPS after Ion Etching. J. Eur. Ceram. Soc. 18 (1998) 339-343.

[32] P. J. Schmitz, Characterization of the Surface of $BaCO_3$ Powder by XPS. Surf. Sci. Spectra 8 (2001) 190-194.

[33] D. Bialuschewski, J. S. Hoppius, R. Frohnhoven, M. Deo, Y. Gönüllü, T. Fischer, E. L. Gurevich, S. Mathur, Laser-Textured Metal Substrates as Photoanodes for Enhanced PEC Water Splitting Reactions. Adv. Eng. Mater. 20 (2018) 1800167.

[34] B. M. Weiss, N. Artioli, E. Iglesia, Catalytic NO Oxidation Pathways and Redox Cycles on Dispersed Oxides of Rhodium and Cobalt. ChemCatChem 4 (2012) 1397-1404.

[35] H. Jin, Y. Huang, J. Jian, Plate-like Cr_2O_3 for highly selective sensing of nitric oxide, Sens. Actuators B Chem 206 (2015)107–110

[36] S. Zhuiykov, T. Nakano, A. Unimoto, N. Yamazoe, N. Miura Potentiometric NO_x sensor based on stabilized zirconia and $NiCr_2O_4$ sensing electrode operating at high temperatures, Electrochem. commun. 3 (2001) 97-101

[37] N. Miura, S. Zhuiykov, T. Ono, M. Hasei, N. Yamazoe, Mixed potential type sensor using stabilized zirconia and $ZnFe_2O_4$ sensing electrode for NO_x detection at high temperature, Sens. Actuators B Chem 83 (2002) 222-229

[38] N. Miura, K. Akisada, J. Wang, S. Zhuiykov, T. Ono, Mixed-Potential-Type NOx Sensor Based on YSZ and Zinc Oxide Sensing Electrode**,** Ionics 10 (2004) 1–9

[39] K. Shimizu, K. Kashiwagi, H. Nishiyama, S. Kakimoto, S. Sugaya , H. Yokoi, A. Satsum, Impedance metric gas sensor based on Pt and WO_3 co-loaded TiO_2 and ZrO_2 as total NO*x* sensing materials, Sens. Actuators B Chem 130 (2008) 707–712

[40] T. Ishihara, H. Fujita, Y. Takita, Effects of Pt addition for $SrSnO_3$–WO_3 capacitive type sensor on NO detection at high temperature Sens. Actuators B Chem 52 (1998) 100–106

[41] P. Tao, Y. Xu, Y. Zhou, C. Song, Y. Qiu, W. Dong, M. Zhang, M. Shao, Nitrogen Oxide (NO) Gas-Sensing Properties of Bi_2MoO_6 Nanosheets Synthesized by a Hydrothermal Method, Mater. Res 20 (2017) 786-790.

[42] M.-R. Wu, W.-Z. Li, C.-Y. Tung, C.-Y. Huang, Y.-H. Chiang, P.-L. Liu, R.-H. Horng, NO gas sensor based on $ZnGa_2O_4$ epilayer grown by metalorganic chemical vapor deposition, Sci. Rep. 9 (2019) 7459.

[43] C. Zhang, G. Liu, X. Geng, K. Wu, M. Debliquy. Metal oxide semiconductors with highly concentrated oxygen vacancies for gas sensing materials: a review. Sens. Actuator A Phys. 309, (**2020)** 112026, doi:10.1016/j.sna.2020.112026.

[44] Y.V. Kaneti, J. Yue, J. Moriceau, C. Chen, M. Liu, Y. Yuan, X. Jiang, A. Yu, Experimental and theoretical studies on noble metal decorated tin oxide flower-like nanorods with high ethanol sensing performance. Sens. Actuators B Chem 219 (2015) 83-93.

[45] C. Liu, Q. Ma, H. He, G. He, J. Ma, Y. Liu, Y. Wu, Structure–activity relationship of surface hydroxyl groups during NO_2 adsorption and transformation on TiO_2 nanoparticles. Environ. Sci. Nano 4 (2017) 2388–2394.

[46] A. Ponzoni, C. Baratto, N. Cattabiani, M. Falasconi, V. Galstyan, E. Nunez-Carmona, F. Rigoni, V. Sberveglieri, G. Zambotti, D. Zappa, Metal Oxide Gas Sensors, a Survey of Selectivity Issues Addressed at the SENSOR Lab, Brescia (Italy). Sensors 17 (2017) 714.

[47] R. Lontio Fomekong and B. Saruhan, Influence of Humidity on NO2-Sensing and Selectivity of Spray-CVD Grown ZnO Thin Film above 400 °C, Chemosensors 7 (2019), 42.